Solid–fluid equilibria for quadrupolar hard dumbbells via Monte Carlo simulation

C. Vega
Departamento de Quimica-Fisica, Facultad de Ciencias Quimicas, Universidad Complutense, 28040 Madrid, Spain

P. A. Monson
Department of Chemical Engineering, University of Massachusetts, Amherst, Massachusetts 01003

(Received 19 July 1994; accepted 4 October 1994)

Solid–fluid equilibrium for the quadrupolar hard dumbbell model has been determined by Monte Carlo simulation for several values of the quadrupole moment and molecular elongation. Several solid structures have been studied including α-N_2, a fcc plastic crystal, based centered monoclinic structure providing closest packing for hard dumbbells and two orthorhombic structures. For low elongations, hard dumbbells freeze into a plastic crystal phase when the quadrupole moment is low and into the α-N_2 structure when it is large. More elongated dumbbells freeze into a close-packed structure for low quadrupole moment, into an orthorhombic structure for moderate quadrupole moment and into the α-N_2 structure for large quadrupole moment. For any elongation and quadrupole moment the stable phase at very high pressures is one of the close-packed structures. The quadrupolar hard dumbbell model gives a qualitatively correct description of trends in the solid–fluid equilibrium for several systems including N_2, the halogens, CO_2, and acetylene. © *1995 American Institute of Physics.*

I. INTRODUCTION

In recent work the phase diagram for the hard dumbbell model has been determined from Monte Carlo simulation studies as a function of the dumbbell bond length.[1–3] This work has revealed several interesting aspects of the role of molecular shape in determining solid–fluid equilibrium. Mildly anisotropic hard dumbbells freeze into a plastic crystal (PC) structure with orientational disorder whereas more anisotropic dumbbells freeze into monoclinic structures that provide the closest packing. The α-N_2 structure which appears in a number of linear molecules (N_2, CO_2, C_2H_2) was not found to be thermodynamically stable for hard dumbbells. When used in a generalized van der Waals theory[4] the results for hard dumbbells provide a qualitative basis for understanding the solid–fluid equilibria for nonpolar diatomic molecules. This illustrates the importance of the packing effects associated with molecular shape in determining solid phase properties and solid–fluid equilibrium.

Of course it is to be expected that other anisotropic forces, such as dispersion and multipolar interactions play an important role in explaining the stability of some solid phases with respect to others. Multipolar forces[5] arising from the presence of a multipolar moment (e.g., dipole or quadrupole) are quite sensitive to the relative orientation between a pair of molecules in the solid phase. Dispersion forces although important seem to be less sensitive to the relative orientation between molecules. In fact Kihara[6] was able to explain the solid structures of several molecules by using hard nonspherical quadrupolar models.

In this work we study the solid–fluid equilibrium of hard dumbbells with an embedded point quadrupole using Monte Carlo simulation. The choice of this model was motivated by the fact that a clear picture of the freezing of nonpolar hard dumbbells has already been developed.[1–3] The effect of the quadrupole moment on the phase diagram can be observed by comparing the results for the quadrupolar hard dumbbell model with those for the hard dumbbell model without the quadrupole. The results should then provide some insight into the phase diagrams of homonuclear diatomic molecules such as N_2, O_2, Cl_2, and Br_2 as well as other quadrupolar molecules such as acetylene and CO_2. We have also studied the phase diagram for the quadrupolar hard sphere model because of its importance as a limiting case.

There has recently been an increasing interest in the theoretical determination of fluid–solid equilibrium of molecular fluids. Density functional theories[7,8] and cell theory[9,4] have been developed to predict the fluid–solid transition of hard dumbbells and comparison with simulation results has been presented. This work provides Monte Carlo data for the fluid–solid equilibrium of hard quadrupolar dumbbells which may be useful to further test these theories so that their predictive value may be compared.

The paper is arranged as follows. In Sec. II the simulation methodology is described. In Sec. III results are presented for a number of models. Section IV gives a summary of our results and conclusions.

II. METHODOLOGY

The interaction between hard dumbbells with an embedded quadrupole along the molecular axis (HDQ) is given by

$$u^{\mathrm{HDQ}}(1,2)=u^{\mathrm{HD}}(1,2)+u^{Q}(1,2), \tag{1}$$

where $u^{\mathrm{HD}}(1,2)$ is the pair potential between hard dumbbells and u^{Q} is the quadrupolar interaction which is given by

$$u^{Q}(1,2)=\frac{3Q^2}{4r^5}\,[1-5(c_1^2+c_2^2)-15c_1^2c_2^2 + 2(s_1s_2c-4c_1c_2)^2], \tag{2}$$

 0021-9606/95/102(3)/1361/12/$6.00

TABLE I. MC results for the fluid phase EOS of quadrupolar hard dumbbells. $L^*=L/\sigma$, $Q^{*2}=Q^2/(kTd^5)$. The parameters k_1, k_2, and k_3 of Eq. (6) obtained from a least squares fit are given.

L^*	Q^{*2}	k_1	k_2	k_3
0	0.5	0.326 9469	0.974 5606	0.612 2980
0	1	−0.743 1447	−0.409 5283	5.231 681
0	1.5	−1.055 726	−3.193 744	8.879 604
0.3	0.3	0.919 6625	1.223 351	−1.210 996
0.3	1.0	−2.266 356	9.405 792	−7.978 440
0.6	0.5	0.928 5581	1.219 304	0.105 0713
0.8	0.2	2.276 923	−0.812 6462	2.176 273
0.8	1.0	0.458 0269	−0.771 7791	4.777 466

where Q is the quadrupole moment, r the distance between the centers of mass, $c_i=\cos(\theta_i)$, $s_i=\sin(\theta_i)$, and $c=\cos(\phi_1-\phi_2)$. Here θ_i and ϕ_i denote the usual orientation angles in the intermolecular frame. The polar axis is the one which connects the centers of mass of the molecules. The geometry of the hard dumbbell is described by $L^*=L/\sigma$ where L is the distance between the two hard spheres of the molecule and σ is the diameter of the hard sphere. In this work the quadrupolar potential given by Eq. (2) has been truncated at $r_c=2.5\sigma$.

In order to determine the phase equilibria, the equation of state (EOS) and chemical potential must be determined in the fluid and solid phases. In the fluid phase we performed standard isobaric, isothermal Monte Carlo (MC) simulations[10] using 108 molecules in a cubic simulation cell with periodic boundaries. The length of runs in this work for fluid and solid phases was typically about 20 000 cycles for equilibration and 20 000 cycles for averages—a cycle consisting of an attempted move for each molecule and an attempted volume change. Fluid runs were started at low pressures and then higher pressures states were obtained from a gradual compression of the final configuration of the previous run.

In this paper we will use reduced variables for the density and quadrupole moment. The reduced density ρ^* is defined as

$$\rho^*=\rho d^3, \tag{3}$$

where ρ is the number density and d is the diameter of the sphere with the same volume as the hard dumbbell

$$d^3=\sigma^3(1+1.5L^*-0.5L^{*3}). \tag{4}$$

The reduced quadrupole is defined as

$$Q^{*2}=\frac{Q^2}{kTd^5}. \tag{5}$$

The compressibility factor of the fluid was fitted to the expression

$$Z=\frac{1+k_1y+k_2y^2+k_3y^3}{(1-y)^3}, \tag{6}$$

where y is the volume fraction. The parameters k_1, k_2, and k_3 were determined through a least-squares fit. Table I gives the values for the coefficients in Eq. (3) which provide the best fit to our fluid phase equation of state results. The Helmholtz free energy of the fluid phase may be obtained from the relation

$$A/NkT=[\ln\rho^*-1]+\int_0^{\rho^*}\frac{Z-1}{\rho^{*\prime}}\,d\rho^{*\prime}, \tag{7}$$

where the term in brackets on the right-hand side of Eq. (7) corresponds to the ideal gas contribution to the Helmholtz free energy, and the integral corresponds to the residual part.

We now describe the simulation methodology for the solid phases. In this work several solid structures have been considered. The first structure studied was the α-N_2 structure. The Bravais lattice for this structure is simple cubic.[11] In this structure the centers of mass of the molecules are arranged on a cubic fcc lattice and the molecules are oriented along the four body diagonals of the cube. The α-N_2 structure does not provide an efficient way of packing for hard dumbbells and in fact it was proved to be thermodynamically unstable for nonpolar hard dumbbells.[2] However it is a common structure for solids of strongly quadrupolar linear molecules and therefore it seems appropriate to consider it for the quadrupolar hard dumbbell model. Second we have considered the base centered monoclinic structures that provide closest packing for hard dumbbells. They are denoted as CP1, CP2, and CP3 and details about their structure are given in Ref. 2. For hard dumbbells these structures were found to be stable[2,3] for densities down to the melting point for $L^*>0.38$. For $L^*<0.38$ they were found to be stable at high pressures. Free energies of the CP1, CP2, and CP3 phases are quite similar, the differences being smaller than the uncertainty of the free energy calculations.[2] However, it could be the case that the free energy differences are increased by the presence of the quadrupole and we shall return to this point later. Another structure considered in this work is a fcc plastic crystal (PC). In this phase the centers of mass of the molecules are arranged in a fcc cubic lattice but there is no long range orientational order. This phase is obtained by expansion of the α-N_2 solid structure (see Ref. 2 for details). Finally we have also considered two orthorhombic structures which will be denoted as O1 and O2. O1 is the structure of the solid halogens[11–13] (Cl_2, Br_2, I_2). The structures are illustrated schematically in Fig. 1. If we label the base vectors of the unit cell as **a**, **b**, and **c** then for O1 the molecular axes all lie in planes parallel to the **a**–**c** plane. O2 is similar to O1 but it differs in that alternate molecules have their axes rotated in and out of the plane parallel to the **a**–**c** plane as shown in Fig. 1. The Bravais lattice for O2 is simple orthorhombic and there are 4 molecules per unit cell. This O2 structure may be considered as a distorted version of the α-N_2 structure.

To simulate the solid phase we used the MC equivalent of the molecular dynamics method developed by Parrinello and Rahman.[14] The method is a constant pressure MC simulation but changes in the unit cell shape are allowed in addition to the volume changes used in the conventional constant pressure MC.[15] The cell shape changes are important because the equilibrium cell shape may change with pressure. For the CP1, CP2, and CP3 structures 144 molecules were used in

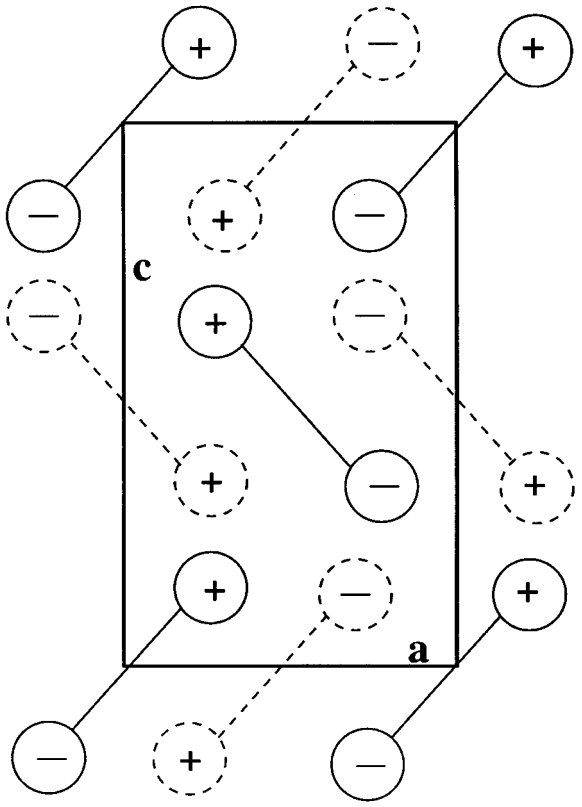

FIG. 1. The orthorhombic structures O1 and O2 viewed in the direction normal to the **a**–**c** plane. In the O1 structure the molecular axes lie in planes parallel to the **a**–**c** plane. The + and − labels on the atoms indicate rotation out of the planar parallel to the **a**–**c** plane in the O2 structure.

the simulations. For the α-N_2, PC, O1, and O2 structures 108 molecules were used. Other details of the simulations are similar to those of our previous work.[2,3]

Once the EOS for a solid phase is known free energy calculations for one thermodynamic state of that solid must be performed so that chemical potential and phase equilibria can be determined. To that purpose we used the Frenkel–Ladd[16] method as extended to nonspherical particles by Frenkel *et al.*[17,18] In this method the free energy of the solid is related to that of an ideal classical Einstein crystal. We refer to the papers of Frenkel *et al.*[17,18] and to our previous work[2,3] for details. The final expression for the Helmholtz free energy of the HDQ solid at a given density is

$$\frac{A}{NkT}=\frac{A_E}{NkT}+\frac{\Delta A_1}{NkT}+\frac{\Delta A_2}{NkT}+\frac{\Delta A_3}{NkT}, \tag{8}$$

where A_E is the free energy of an ideal Einstein crystal and ΔA_1 is the difference between the free energy of an ideal Einstein crystal and that of an Einstein crystal with HDQ interactions. ΔA_2 is the difference between the free energy of the HDQ solid and that of an Einstein crystal with HDQ interactions, and ΔA_3 is the difference in free energy between a system of unconstrained center of mass and one of fixed center of mass. The expressions used for A_E, ΔA_2, and ΔA_3 are identical to those given in Ref. 2. The expression for ΔA_1 however is slightly different for the HDQ than for the HD system. The ΔA_1 for HDQ is obtained from the relation

$$\Delta A_1/NkT=-\frac{1}{N}\ln\left\langle \exp\left[-\beta\sum_{i<j}u^{\mathrm{HDQ}}(i,j)\right]\right\rangle, \tag{9}$$

where the brackets denote canonical ensemble average over configurations generated according to the canonical distribution function of the noninteracting Einstein crystal. The $\Delta A_1/NkT$ term is comparable in magnitude to the quadrupolar internal energy of the solid U^Q/NkT. Whereas for HD, $\Delta A_1/NkT$ was always positive and small, in the HDQ system the sign of $\Delta A_1/NkT$ is that of the quadrupolar internal energy. The evaluation of $\Delta A_1/NkT$ given by Eq. (9) was performed by using umbrella sampling.

In the evaluation of the free energy we used the equilibrium geometry of the unit cell resulting from the MC runs. This allows for any change in the lattice geometry that may occur in the expansion from close packing. Once the free energy of a given HDQ solid structure has been determined for a given density then free energies at other densities can be determined by thermodynamic integration

$$A(\rho_2)/NkT=A(\rho_1)/NkT+\int_{\rho_1}^{\rho_2}[p/(\rho^2kT)]d\rho. \tag{10}$$

To perform integration in Eq. (10) we fitted the pressure of the solid to a polynomial in density. At high pressures the logarithm of the pressure was fitted to a polynomial form in density.

We have checked our solid phase free energy calculations for thermodynamic consistency. For that purpose we have evaluated the free energy of the α-N_2 lattice for $L^*=0.3$ and $Q^{*2}=0.3$ at two different densities ($\rho^*=1.2120$ and $\rho^*=1.3500$) with the Frenkel–Ladd method and in this way we found a free energy difference of $\Delta A/NkT=3.31$. By integration of the equation of state we found that $\Delta A/NkT=3.28$ which indicates that the two calculations are thermodynamically consistent within the accuracy of our calculations.

III. RESULTS AND DISCUSSION

MC results for the solid phase properties obtained for $L^*=0.0$, 0.3, 0.6, and 0.8 and several values of Q^{*2} are shown in Tables II–V. Free energy calculations for the solid phases are presented in Table VI. The computed phase transitions are shown in Table VII. The estimated uncertainties are about 1% for the solid phase densities and about 6% for the quadrupolar energies. We shall proceed now to separate discussion of the results for each dumbbell elongation.

A. Results for $L^*=0$

For $L^*=0$ the HDQ model reduces to a hard sphere with an embedded point quadrupole, and the results for this system can be compared with those for hard spheres.[19] For $L^*=0$ the α-N_2 and CP structures have the same close packing density, $\rho^*=2^{1/2}$. However, the orientations of the molecules in the solid (given by the orientation of the quadrupole) are quite different. In Table VIII the internal energy at close packing is given for the α-N_2 and CP structures for

TABLE II. MC results for α-N_2 solid structure of quadrupolar hard spheres ($L^*=0$). $p^*=p/(kT/d^3)$, $\rho^*=\rho d^3$, U^Q is the quadrupolar internal energy and S denotes the orientational order parameter as defined in Ref. 2. The quadrupolar potential was truncated at $r_c=2.5\sigma$ except for states labeled with an asterisk where the value $r_c=2.9\sigma$ was used. Low values of $S\sim 1/9$ indicate the appearance of a plastic crystal phase.

Q^{*2}	p^*	ρ^*	$U^Q/(NkT)$	S
0.5	60	1.327	−3.61	
	45	1.313	−3.31	
	40	1.302	−3.41	
	35	1.288	−3.37	
	30	1.266	−3.24	
	25	1.249	−3.04	
	20	1.217	−2.91	
	15	1.162	−2.42	
	12.5	1.120	−1.67	
	10	1.037	−1.35	
0.5	60*	1.330	−3.52	0.74
	45*	1.310	−3.46	0.64
	40*	1.299	−3.38	0.48
	35*	1.290	−3.32	0.37
	30*	1.278	−3.25	0.28
	25*	1.254	−3.03	0.14
	20*	1.217	−2.77	0.11
	15*	1.156	−2.26	0.11
	12.5*	1.113	−1.55	0.10
	10*	1.039	−1.34	0.11
1.0	45	1.326	−8.51	0.92
	40	1.318	−8.42	0.92
	30	1.292	−8.12	0.91
	20	1.269	−7.84	0.91
	15	1.244	−7.56	0.90
	12.5	1.227	−7.37	0.90
	10	1.206	−7.13	0.90
	8	1.177	−6.81	0.88
	6	1.150	−6.50	0.88
	4	1.084	−5.82	0.80
	3	1.041	−5.36	0.57
1.5	40	1.330	−13.39	0.95
	30	1.314	−13.11	0.94
	20	1.294	−12.77	0.93
	15	1.281	−12.55	0.93
	10	1.269	−12.34	0.93
	8	1.259	−12.17	0.92
	6	1.237	−11.79	0.89
	4	1.232	−11.72	0.89
	2	1.214	−11.38	0.87
	1	1.199	−11.17	0.88
	0.75	1.184	−10.90	0.87
	0.5	1.199	−11.16	0.88

$Q^{*2}=1$. The quadrupole favors the α-N_2 structure which has a negative value of U^Q/NkT relative to the CP structures which have positive values. It is interesting to note that CP1, CP2, and CP3 have quite similar values of U^Q/NkT for all elongations so that the quadrupole does not favor a given close packed structure over the others. This suggests that the α-N_2 structure is likely to be the stable one for quadrupolar hard spheres.

In Table II our simulation results for the α-N_2 solid phase with $Q^{*2}=0.5$, 1, 1.5 are presented. Although no systematic study of the effect of truncating the quadrupolar interaction has been performed we have made some additional calculations with $r_c=2.9\sigma$ for 256 molecules. For the 108 molecule systems the cutoff of 2.5 σ is slightly larger than half the box length for the solid phases with $L^*=0$ (but not for the other values of L^* considered in this work) and since periodic boundaries with the minimum image criterion were used there is a slight anisotropy in the truncation of the potential in this case. For the systems with a cutoff of 2.9 σ this does not occur because of the larger system size. Although some differences between the two sets of results are evident it seems that these differences are comparable to the statistical uncertainty in the results. Notice that the orientational order parameter[2] decreases smoothly with pressure. The orientational order parameter used in this work varies between unity for a system with the orientational order of the initial lattice and $\sim 1/9$ for an orientationally disordered state. The lower pressure states for $Q^{*2}=0.5$ correspond to a plastic crystal phase (PC). The transition to the PC phase appears to be second order. The PC with $Q^{*2}=0.5$ exhibits a high degree of orientational disorder at melting. Solid–fluid equilibria for $L^*=0$ and $Q^{*2}=0.5$, 1, 1.5 are presented in Table VII. In Fig. 2(a) results are shown for the cases $Q^{*2}=0.5$ and 1.0. The quadrupole decreases the pressure of the fluid–solid transition with respect to the hard sphere case. The effect is small for $Q^{*2}=0.5$ and large for $Q^{*2}=1$. This is due to the fact that for $Q^{*2}=0.5$ the solid phase is a PC, whereas for $Q^{*2}=1.5$ the solid phase presents a large degree of orientational order. The fluid density at coexistence decreases with the quadrupole moment but the density change on freezing increases. In Fig. 2(b) coexistence densities of the fluid–solid equilibria of quadrupolar hard spheres are shown. The reduced temperature is defined as $T^*=kTd^5/Q^2$. Notice that this system does not seem to exhibit a vapor–liquid critical point. In this regard it is quite similar to other systems with weakly attractive or short range forces which have been studied recently.[20–22]

B. Results for $L^*=0.3$

For $L^*=0.3$ we have studied systems with $Q^*=0.3$ and $Q^*=1$. Results are presented in Table III. We shall first discuss the $Q^{*2}=0.3$ case. At very high pressures the close packed structures are stable. This can be understood from the fact that the pressure of the α-N_2 phase diverges when the density tends to $\rho^*=1.4657$, the maximum possible density of hard dumbbells with this structure for this elongation. The CP structures exhibit this divergence when ρ^* tends to $\rho^*=1.4917$. This kind of divergence was analyzed in detail by Alder, Hoover, and Young for the hard sphere case.[23] According to the cell theory[23,24] the origin of this divergence is the fact that the free volume of each molecule tends to zero at close packing, so that free energy and pressures diverge. Therefore whenever the maximum allowed density of a given structure is approached the free energy diverges and a transition to another structure which packs molecules more efficiently is expected. At very high pressures the CP structures should be the stable phases. The differences between the free energies of the CP structures are small and we cannot establish which is the most stable among them. It can be seen from the results of Table III that the EOS for the CP1

TABLE III. MC results for different solid structures of quadrupolar hard dumbbells with $L^*=0.3$. Notation as in Table I. Values of pressure labeled with an asterisk where obtained by compressing the PC solid. Values of pressure followed by the name of a structure in brackets indicate the spontaneous formation of that phase by expansion of the α-N_2 or compression of the PC phase.

Q^{*2}	Solid	p^*	ρ^*	$U^Q/(NkT)$	Q^{*2}	Solid	p^*	ρ^*	$U^Q/(NkT)$
0.3	CP3	1000	1.481	3.14	0.3	PC	17*	1.072	−0.71
		500	1.470	3.10			18*	1.087	−0.74
		300	1.453	3.00			19*	1.099	−0.79
		200	1.437	2.88			20*	1.110	−0.82
		150	1.417	2.71			21*	1.113	−0.82
		100	1.375	2.30			22*	1.140	−1.19
		80	1.330	1.29			23*(α-N_2)	1.196	−1.92
		70	1.293	−0.19			24*(α-N_2)	1.203	−1.98
		60	1.272	−0.64			25*(α-N_2)	1.227	−2.12
0.3	CP1	1000	1.481	3.13			30*(α-N_2)	1.247	−2.23
		500	1.470	3.09	1.0	α-N_2	1000	1.456	−11.17
		300	1.455	3.01			500	1.447	−11.05
		200	1.436	2.87			300	1.437	−10.91
		150	1.412	2.60			200	1.426	−10.75
		100	1.372	2.20			100	1.398	−10.30
0.3	α-N_2	1000	1.455	−3.35			80	1.386	−10.12
		500	1.447	−3.31			25	1.302	−8.84
		300	1.435	−3.26			20	1.280	−8.52
		200	1.421	−3.20			15	1.261	−8.25
		100	1.387	−3.03			12.5	1.243	−8.00
		80	1.366	−2.91			10	1.228	−7.80
		70	1.353	−2.84			7.5	1.186	−7.27
		60	1.338	−2.77			5	1.132	−6.62
		50	1.322	−2.67			4	1.114	−6.42
		45	1.310	−2.59	1.0	CP3	1000	1.481	10.39
		40	1.297	−2.53			500	1.470	10.13
		35	1.270	−2.37			300	1.449	9.36
		30	1.249	−2.24			200	1.405	5.68
		25	1.219	−2.04					
		24	1.208	−1.99					
		23	1.196	−1.91					
		22	1.185	−1.85					
		21	1.178	−1.80					
		20	1.148	−1.53					
		19	1.137	−1.46					
		18(PC)	1.102	−0.81					
		17(PC)	1.077	−0.73					
		16(PC)	1.062	−0.69					
		15(PC)	1.103	−0.77					
		14(PC)	1.044	−0.66					
		13(PC)	1.018	−0.60					
		12(PC)	0.977	−0.55					

and CP3 are almost identical. In the rest of this work we shall take the CP3 structure as representative of all CP structures anticipating that the behavior of CP1 and CP2 should be quite similar. As the pressure is decreased there is a crossing between the EOS of the α-N_2 and that of the CP3 structure. We performed free energy calculations for both structures and found a transition from CP3 to α-N_2 as the pressure was decreased. The origin of this transition is the competition between the repulsive forces from the molecular shape which favor the CP structure and the quadrupolar forces which favor the α-N_2 structure. Packing considerations must dominate at high pressure whereas the quadrupolar forces can stabilize the α-N_2 structure at low pressure.

By further expanding the α-N_2 structure a significant change occurs at $p^*=18$. The orientational order parameter,

TABLE IV. MC results for different solid structures of quadrupolar hard dumbbells with $L^*=0.6$. Notation as in Table I.

Q^{*2}	Solid	p^*	ρ^*	$U^Q/(NkT)$	Solid	p^*	ρ^*	$U^Q/(NkT)$
0.5	α-N_2	100	1.337	−4.78	CP3	100	1.378	3.16
		80	1.323	−4.68		80	1.335	1.68
		70	1.312	−4.61		70	1.313	−0.73
		60	1.301	−4.54		60	1.293	−1.36
		40	1.260	−4.25		45	1.238	−0.92
		35	1.252	−4.19		40	1.219	−1.52
		30	1.232	−4.05		35	1.189	−1.96
		25	1.217	−3.95		30	1.158	−2.25
		20	1.180	−3.68		25	1.125	−2.40
		15	1.121	−3.26				
		12.5	1.065	−2.89				
		10	1.012	−2.52				

TABLE V. MC results for different solid structures of quadrupolar hard dumbbells with $L^*=0.8$. Notation as in Tables I and IV. Considered solid structures are α-N_2, CP3, O2 and the experimental structure of halogens O1. Lengths (in σ units) of the simulation box denoted as a, b and c are shown at some states. The lengths of the unit cell base vectors can be obtained by dividing a, b, and c by three.

Q^{*2}	Solid	p^*	ρ^*	$U^Q/(NkT)$	a	b	c
0.2	CP3	100	1.370	0.66			
		80	1.345	0.62			
		70	1.332	0.60			
		60	1.306	0.56			
		50	1.273	0.50			
		45	1.255	0.47			
		40	1.231	0.39			
		35	1.204	0.36			
		30	1.162	0.31			
		25	1.107	0.02			
0.2	α-N_2	50	1.204	−1.58	5.60	5.55	5.61
		45	1.196	−1.56	5.50	5.63	5.67
		42.5	1.196	−1.55	5.44	5.55	5.81
		40	1.204	−1.56	5.27	5.51	6.00
		37.5	1.217	−1.57	5.11	5.49	6.15
		35(O2)	1.205	−1.54	5.12	5.53	6.15
		30(O2)	1.185	−1.48	5.11	5.59	6.21
		25(O2)	1.130	−1.35	5.20	5.73	6.23
		20(O2)	1.072	−1.17	5.25	5.85	6.38
		19(O2)	1.080	−1.17	5.15	5.79	6.52
		18(O2)	1.045	−1.03	5.08	5.91	6.68
		17(O2)	1.021	−0.97	5.16	5.97	6.68
		16(O2)	1.001	−0.88	5.26	6.00	6.65
0.2	O2	30	1.174	−1.46	5.09	5.63	6.23
		35	1.202	−1.51	4.93	5.65	6.27
		40	1.224	−1.58	5.00	5.52	6.20
		45	1.246	−1.64	5.02	5.46	6.15
		50	1.257	−1.67	4.96	5.47	6.14
		60	1.280	−1.73	4.94	5.44	6.10
		70	1.302	−1.79	4.96	5.38	6.04
		80	1.313	−1.82	4.96	5.33	6.03
		100	1.336	−1.88	4.95	5.29	5.98
0.2	O1	50	1.244	−0.63	3.92	4.95	8.70
		45	1.241	−0.83	4.05	4.89	8.52
		40	1.217	−0.82	4.14	4.91	8.49
		35	1.196	−0.84	4.20	4.97	8.41
		30	1.155	−0.80	4.27	5.07	8.40
		25	1.122	−0.81	4.42	5.13	8.25
		20	1.041	−0.70	4.69	5.47	7.86
1	α-N_2	150	1.291	−9.08	5.44	5.45	5.49
		100	1.272	−8.85	5.46	5.47	5.52
		80	1.264	−8.74	5.41	5.52	5.56
		60	1.249	−8.56	5.38	5.52	5.65
		40	1.276	−8.68	5.03	5.42	6.04
		30(O2)	1.252	−8.37	5.07	5.44	6.08
		20(O2)	1.193	−7.69	5.17	5.56	6.12
		10(O2)	1.105	−6.70	5.35	5.76	6.20
		8(O2)	1.043	−6.02	5.52	5.89	6.20
		6(O2)	1.021	−5.79	5.57	5.96	6.19
		4(O2)	0.934	−4.84	5.91	6.13	6.21
		40(O2)	1.276	−8.67	5.02	5.41	6.07
		50(O2)	1.297	−8.92	4.98	5.38	6.04
		60(O2)	1.311	−9.09	4.96	5.36	6.03
		80(O2)	1.327	−9.28	4.95	5.31	6.01
		100(O2)	1.349	−9.56	4.94	5.28	5.97
		150(O2)	1.371	−9.83	4.92	5.24	5.94
		300(O2)	1.397	−10.15	4.91	5.20	5.90

TABLE V. (*Continued*.)

Q^{*2}	Solid	p^*	ρ^*	$U^Q/(NkT)$	a	b	c
1	α-N_2	30	1.193	−7.85	5.52	5.60	5.69
		20	1.159	−7.43	5.60	5.60	5.77
		10	1.083	−6.51	5.84	5.79	5.73
		8	1.066	−6.32	5.74	5.83	5.88
		6	1.013	−5.72	5.98	5.98	5.80
		5	0.993	−5.51	5.93	6.05	5.90
		4	0.969	−5.24	5.98	6.02	6.02
1	CP3	1000	1.460	3.49			
		500	1.450	3.44			
		300	1.433	3.23			
		200	1.413	2.89			
		150	1.393	2.59			
		100	1.344	1.58			
		80	1.301	0.625			

internal energy, and density drop significantly. The α-N_2 phase has transformed into a PC phase which can be further expanded until it spontaneously melts. In order to understand the nature of the transition between the α-N_2 and the PC we carried out a gradual compression of the PC phase obtained at $p^*=17$ from the expansion of the α-N_2 structure. Results of this compression are shown in Table III and in Fig. 3 where it is seen that the compressed PC states lie on a different branch than the α-N_2 states. When $p^*=23$ the PC phase transforms into α-N_2 phase again. The presence of this hysteresis loop is indicative of a first-order phase transition. In fact free energy calculations show a first-order phase transition between the α-N_2 and the PC at $p^*=19.35$. Figure 3 shows the scenario for $L^*=0.3$ and $Q^{*2}=0.3$. The fluid freezes into a PC phase that is unstable with respect to the α-N_2 structure at higher densities and with respect to a monoclinic base centered structure (CP3) at even higher pressures. By comparing with the phase diagram of HD with $L^*=0.3$ it is concluded that the effect of a quadrupole moment on the phase diagram of HD is to insert a region of stability of the α-N_2 phase between the PC and CP3 phases.

We have also analyzed the phase diagram for $L^*=0.3$ and $Q^*=1$. Results are shown in Table III. At high densities CP3 is again the stable structure. It becomes unstable with respect to the α-N_2 phase at lower pressures. When this α-N_2 structure is further expanded it finally melts when $p^*=4.61$. The phase diagram for $Q^*=1$ is shown in Fig. 4. The most interesting feature is that the PC phase has disappeared. In Ref. 3 it was argued that the maximum allowed anisotropy of hard dumbbells in order to have a PC phase is of $L^*=0.38$. This work shows an additional restriction that there also be a low quadrupole moment.

The results we have obtained for the HDQ models with $L^*=0.3$ permit us to construct a schematic phase diagram as shown in Fig. 5 which summarizes all the available information. At low values of Q^{*2} the fluid freezes into a PC phase which becomes unstable with respect to a CP structure at higher pressures. For moderate Q^{*2} values the fluid freezes into a PC phase. This becomes unstable with respect to the α-N_2 phase at higher pressures and into a CP structure at still higher pressures. For high quadrupole moments the

TABLE VI. Free energy calculations for different solid structures of quadrupolar hard dumbbells. Notation as in preceding tables. λ is the maximum value of λ used in the free energy calculations. ΔA_1 is given by Eq. (9) of this work and ΔA_2 is given by Eq. (3.14) of Ref. 2. A_{ref} is the Helmholtz free energy at the reference density. All free energies are divided by NkT.

L^*	Q^{*2}	Lattice	N	$\lambda_{\max}$	ρ^*	ΔA_2	ΔA_1	A_{ref}
0	0.5	PC	108	1000	1.037	−8.8241	−3.1725	4.1903
0	1	α-N_2	108	8000	1.150	−11.4708	−7.5611	2.3262
0	1.5	α-N_2	108	8000	1.200	−10.1726	−12.1749	−0.989
0.3	0.3	PC	108	1000	1.053	−9.2780	−1.9664	5.3015
0.3	0.3	α-N_2	108	8000	1.2120	−11.5148	−2.4827	7.7199
0.3	0.3	α-N_2	108	8000	1.3500	−7.7299	−2.9549	11.034
0.3	0.3	CP3	144	30000	1.4173	−5.11667	2.6954	22.611
0.3	1.0	α-N_2	108	8000	1.1320	−12.0519	−7.3855	2.2794
0.3	1.0	α-N_2	108	8000	1.3500	−7.4371	−9.8887	4.3926
0.3	1.00	CP3	144	90000	1.4481	−7.6815	9.3302	29.417
0.6	0.5	α-N_2	108	8000	1.1210	−12.0550	−3.6702	6.2105
0.8	0.2	O2	108	8000	1.0798	−11.9668	−1.3059	8.7435
0.8	0.2	CP3	144	8000	1.1721	−10.3351	0.2279	11.9336
0.8	1.0	α-N_2	108	8000	1.1300	−10.4600	−7.4389	4.1177
0.8	1.0	O2	108	8000	1.1932	−9.2622	−7.8444	4.9104

fluid freezes into the α-N_2 structure that is unstable with respect to a CP structure at high pressures. It is straightforward to show that the slope of a given phase transition in the units of Fig. 5 is given by

$$(dp^*/dQ^{*2}) = \rho_1^* \rho_2^* [\Delta U/(NkTQ^{*2}\Delta\rho^*)], \tag{11}$$

where $\Delta\rho$ and ΔU are the change in density and configurational energy at the transition. For all the studied transitions $\Delta\rho$ is positive. Therefore the sign of (dp^*/dQ^{*2}) is that of ΔU. The slopes of the lines shown in Fig. 5 are in agreement with this relation.

In Fig. 5 estimated values of $Q^2/(kT_m d^5)$ for N_2 and C_2H_2 are also shown. The experimental[5] quadrupole moment and melting temperature[25] T_m of these two substances have been used along with a reasonable estimation of d.[26,27] It is interesting to note that N_2 freezes into a PC phase (although slightly different from the one obtained in this work). Moreover nitrogen also exhibits the α-N_2 and rhombohedral structures in its experimental phase diagram.[11] The fractional density change at freezing for N_2 is small in agreement with this work and with previous simulation results.[28] Acetylene freezes into an α-N_2 structure[29] in agreement with the model results in Fig. 5.

C. Results for $L^*=0.6$

For $L^*=0.6$ we have studied the model with $Q^{*2}=0.5$. In Table IV results are shown for the α-N_2 and CP3 structures. In Fig. 6 the phase diagram for the model is illustrated. The fluid freezes into an α-N_2 and by compression a phase transition to the CP3 structure is obtained although no attempt to locate the α-N_2 to CP3 transition has been made. For the HD model of the same elongation the fluid freezes into a CP structure. The quadrupole therefore introduces a region of stability of the α-N_2 phase between the fluid and the CP phase.

We have found some interesting results for the quadrupolar energy for the CP3 structure. For this structure U^Q is

TABLE VII. Fluid–solid and solid–solid equilibria of quadrupolar hard dumbbells as determined from the MC results of fluid (Table I) and solid phases (Tables II–V), and from the free energy calculations of Table VI. Notation as in preceding tables.

L^*	Q^{*2}	Phase 1	Phase 2	ρ_1^*	ρ_2^*	p^*	μ/kT
0	0.5	Fluid	PC	0.9505	1.0885	11.09	14.86
0	1	Fluid	α-N_2	0.8175	1.1025	4.43	6.15
0	1.5	Fluid	α-N_2	0.2750	1.1870	0.36	−0.71
0.3	0.30	Fluid	PC	0.996	1.048	14.9	14.44
0.3	0.30	PC	α-N_2	1.103	1.153	19.35	23.59
0.3	0.30	α-N_2	CP3	1.455	1.487	935.14	657.14
0.3	1	Fluid	α-N_2	0.8035	1.1275	4.61	6.36
0.3	1	α-N_2	CP3	1.459	1.486	1741.66	1182.6
0.6	0.5	Fluid	α-N_2	0.9445	1.0785	12.91	17.69
0.8	0.2	Fluid	O2	1.0605	1.1675	28.76	35.00
0.8	0.2	Fluid	CP3	1.1535	1.2565	47.55	51.90
0.8	1	Fluid	α-N_2	0.8045	1.015	5.86	8.99
0.8	1	Fluid	O2	0.819	1.025	6.27	9.49
0.8	1	α-N_2	O2	1.140	1.168	16.50	18.70

TABLE VIII. Quadrupolar internal energy U^Q/NkT of quadrupolar hard dumbbells at close packing for several solid structures. The presented U^Q/NkT values correspond to $Q^{*2}=Q^2/(kTd^5)=1$. ρ_{cp}^{CP} and $\rho_{cp}^{\alpha\text{-}N_2}$ represent the close packing densities of the close packed (CPs) and α-N_2 structures respectively. If no distortion of the unit cell occurs internal energies at different densities and quadrupoles may be obtained by multiplying values on this table by the factor Q^{*2} $(\rho/\rho_{cp})^{5/3}$.

L^*	ρ_{cp}^{CP}	$\rho_{cp}^{\alpha\text{-}N_2}$	CP1 $U^Q/(NkT)$	CP2 $U^Q/(NkT)$	CP3 $U^Q/(NkT)$	α-N_2 $U^Q/(NkT)$
0	1.4142	1.4142	2.658	2.658	2.658	−10.605
0.1	1.4485	1.4452	6.304	6.305	6.276	−10.995
0.2	1.4741	1.4618	9.069	9.073	9.028	−11.206
0.3	1.4917	1.4657	10.777	10.785	10.751	−11.257
0.4	1.5016	1.4585	11.361	11.368	11.352	−11.164
0.5	1.5044	1.4412	10.792	10.791	10.789	−10.944
0.6	1.5001	1.4147	9.099	9.086	9.092	−10.611
0.7	1.4890	1.3797	6.413	6.391	6.397	−10.177
0.8	1.4709	1.3366	2.996	2.970	2.971	−9.652
0.9	1.4461	1.2855	−0.763	−0.785	−0.792	−9.046
1.0	1.4142	1.2266	−4.367	−4.377	−4.395	−8.366

positive at high pressures and becomes negative at low pressures. In fact at close packing U^Q for the CP3 structure is strongly positive (see Table VIII) and on this basis the high pressure behavior of U^Q is easily understood. The quadrupole tends to destabilize the CP structures. The change of sign of U^Q for the CP3 is due to distortion of the unit cell with respect to that at close packing as the pressure is decreased. This distortion affects the parameters of the unit cell and the orientation of the molecules within the unit cell. At close packing the angle θ between the molecular axis and the perpendicular to the ab plane is on average $\theta=20.3°$ whereas when $p^*=35$ this angle is on average $\theta=40.5°$. This change allows a more favorable orientation of the quadrupolar interactions. We already mentioned in our previous work the importance of lattice distortion when computing the free energy of a solid phase.[2] For HD this effect although appreciable was not large. However it becomes very important when polar forces are present. In fact without lattice distortion U^Q would take a value of about $U^Q/NkT=3.09$ when $\rho^*=1.189$ and $Q^{*2}=0.5$ whereas the MC value is $U^Q/NkT=-1.96$. Theoretical treatments of solid phases should therefore consider the possibility of lattice distortion when dealing with quadrupolar interactions. Otherwise important errors in the determination of thermodynamic properties of the solid phase may occur.

Finally, although we have not considered it for this dumbbell bond length an orthorhombic structure may appear as the stable structure on freezing for small values of the quadrupole moment, as we shall see for the case of $L^*=0.80$.

D. Results for $L^*=0.80$

For $L^*=0.8$ the values of the quadrupole considered were: $Q^{*2}=0.2$ and 1.0. For $Q^{*2}=0.2$ results for several solid structures are shown in Table V. The EOS for the CP3 structure has been obtained at high and low pressures. Results for the α-N_2 structure are also presented. The cubic geometry of this structure is preserved in the initial high pressure states. However when pressure is decreased the α-N_2 becomes mechanically unstable and transforms into the orthorhombic structure O2. This structure is clearly visible at pressures smaller than $p^*=35$. When the O2 structure at $p^*=30$ obtained from expansion of the α-N_2 solid is compressed the system follows a different path for $p^*>35$ than the one obtained from expansion of the α-N_2. Therefore this O2 structure is mechanically stable up to very high pressures.

In Fig. 7 the EOS for all the different phases are shown. The EOS of the O2 and the CP3 solids cross for a pressure of about $p^*=35$. That indicates a phase transition from the O2 to the CP3 structure at high pressures. For $Q^{*2}=0.2$ the fluid freezes into an orthorhombic structure O2 and at high

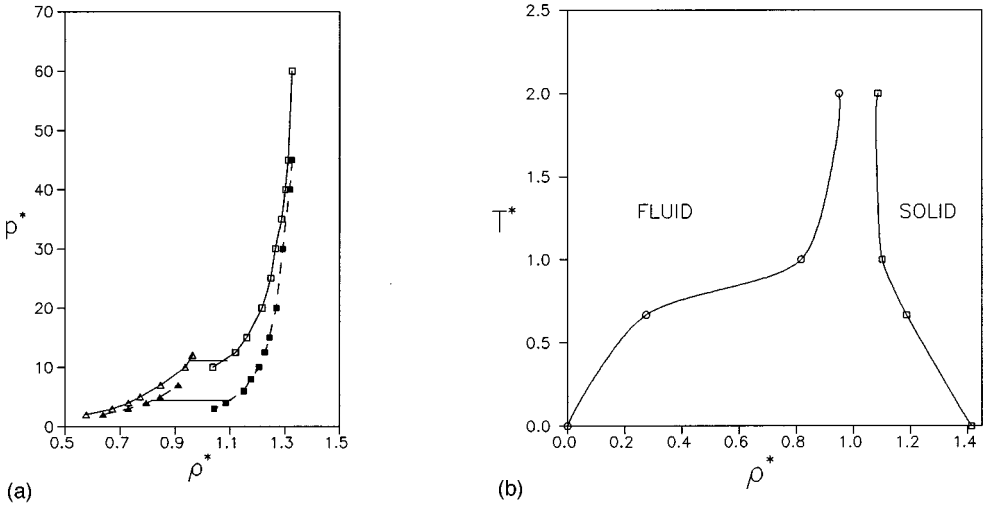

FIG. 2. (a) Equation of state for quadrupolar hard spheres ($L^*=0$) with $Q^{*2}=0.5$ (solid line) and $Q^{*2}=1.00$ (dashed line). Triangles correspond to MC results of the fluid phase for $Q^{*2}=0.5$ (*open*) and $Q^{*2}=1$ (*filled*). Squares correspond to MC results the solid phase for $Q^{*2}=0.5$ (*open*) and $Q^{*2}=1$ (*filled*). Fluid solid transitions are shown by the tie lines. (b) Transition densities for quadrupolar hard spheres. Reduced temperature is defined as $T^*=T/[Q^2/(kd^5)]=1/Q^{*2}$. Results for $T^*=0$ correspond to extrapolation of the results obtained at higher temperatures.

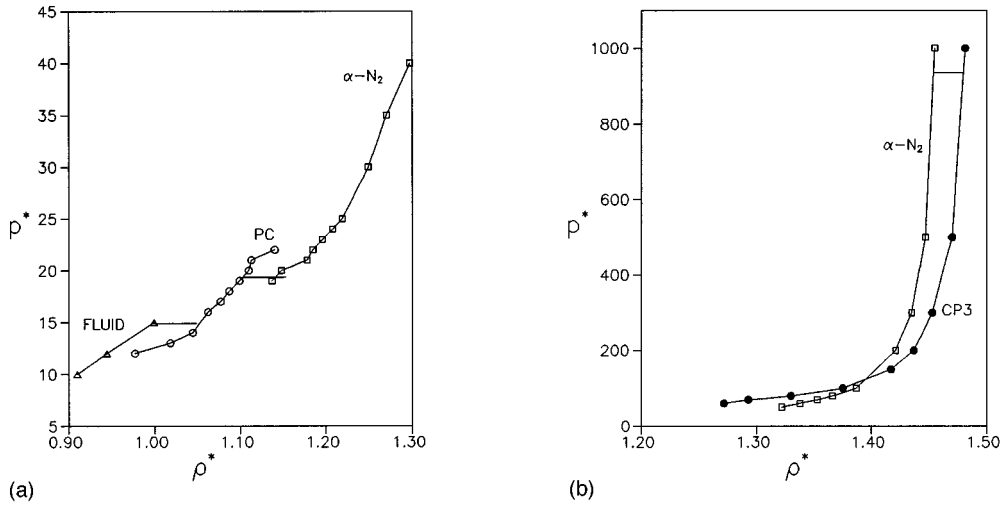

FIG. 3. Equation of state for HDQ with $L^*=0.3$ and $Q^{*2}=0.30$. Symbols stand for MC results: triangles (fluid phase); open circles (plastic crystal PC); squares (α-N_2); filled circles (CP3). The tie lines show the phase transitions (a) low pressure results, (b) high pressure results.

pressures this O2 structure becomes unstable with respect to a close packing (base centered monoclinic) structure (CP3). The α-N_2 phase is absent for this model. The appearance of an orthorhombic structure is a new feature. It appears for elongated molecules with moderate values of the quadrupole moment. It should be recalled that for the corresponding nonpolar HD model with $L^*=0.8$ no orthorhombic phase was found. The conditions for the appearance of orthorhombic phases are elongated molecules with moderate quadrupoles. This is not surprising. In fact Cl_2, Br_2, I_2 (which correspond to values of L^* ranging from 0.6 to 0.8) have orthorhombic structures at freezing.[11] On the basis of static lattice energy summations, English and Venables[30] concluded that for quadrupolar two center Lennard-Jones models the orthorhombic structure was the most stable one for large elongation and moderate quadrupole. This is in agreement with the findings of this work. However it should be pointed out that the orthorhombic structure O2 differs from the experimental orthorhombic (O1) structure found in halogens. To analyze this point further we performed MC simulations of HDQ models by using the O1 structure of halogens. Results are shown in Table VII. Free energy calculations show that for $Q^{*2}=0.2$ this structure is less stable than the O2 solid. We conclude that for this model although an orthorhombic phase appears at freezing it is not identical to that found in real halogens. It seems possible that dispersion forces would favor the O1 structure over the O2 structure.

We now consider the results for $L^*=0.8$ and $Q^*=1$. When starting from an α-N_2 structure at high pressures (see Table V) this structure becomes mechanically unstable and it transforms into the orthorhombic structure O2. When this O2 structure is expanded it finally melts. We also compressed the O2 structure starting from the state at $p^*=40$. These results are shown in Fig. 8(a). Results for the CP3 structure are shown in Table V and in Fig. 8(b). As is shown in Fig.

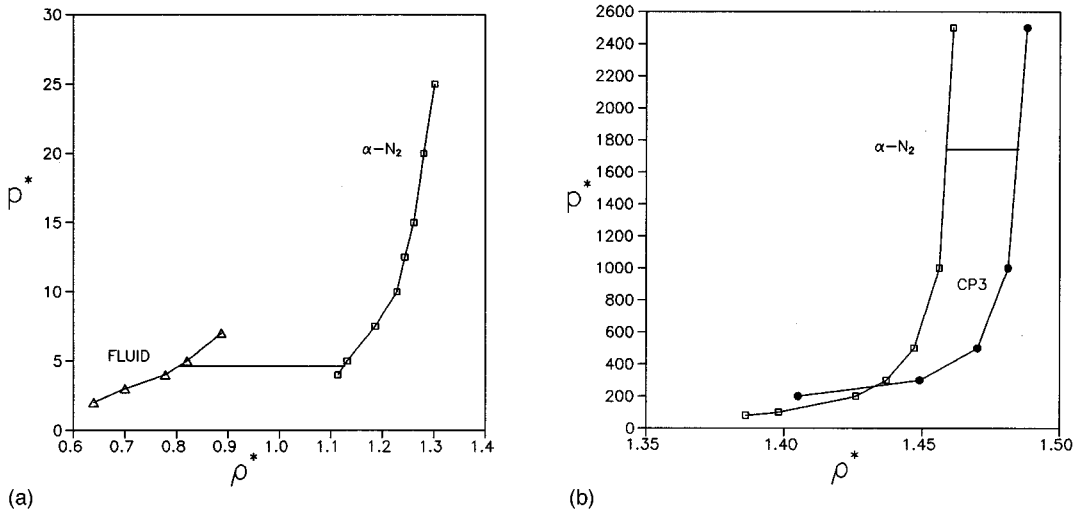

FIG. 4. Equation of state for HDQ with $L^*=0.3$ and $Q^{*2}=1$. Notation as in Fig. 3: (a) low pressure results; (b) high pressure results.

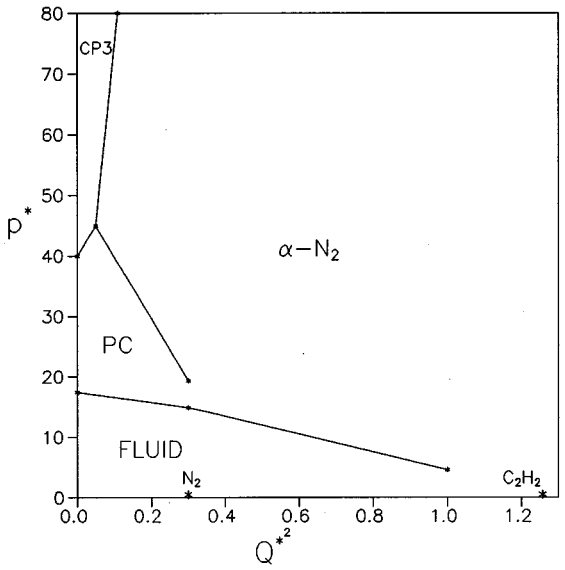

FIG. 5. Phase diagram for quadrupolar hard dumbbells with $L^*=0.3$ for several values of $Q^{*2}=Q^2/(kTd^5)$. Lines correspond to first-order phase transitions. Approximate values of Q^{*2} for N_2 and C_2H_2 at the triple point are indicated.

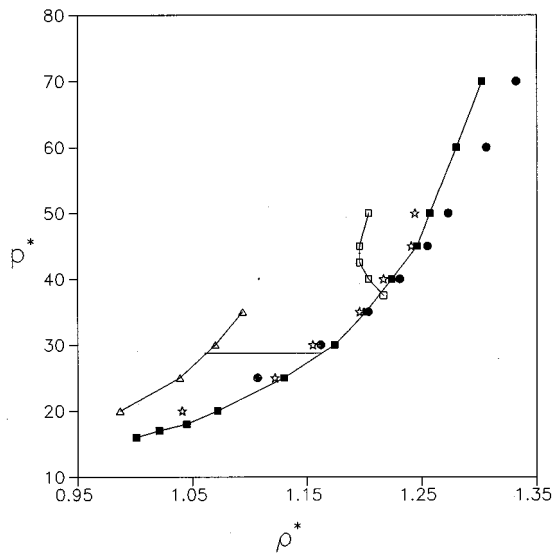

FIG. 7. Equation of state for HDQ with $L^*=0.8$ and $Q^{*2}=0.2$. Symbols stand for MC results: triangles (fluid phase); open squares (α-N_2); filled squares (orthorhombic structure O2); filled circles (CP3); stars (orthorhombic structure O1). The tie lines show the phase transitions.

8(b) there is a crossing between the EOS of the O2 and CP3 structures suggesting the possibility of a phase transition from the O2 to the CP3 at high pressures. So far the results are quite similar to those presented for $Q^{*2}=0.2$ and $L^*=0.8$. However there is an important difference. We performed free energy calculations at lower pressure and found the α-N_2 structure to be more stable than the O2 structure at melting. According to the results of this work for this model the fluid freezes into the α-N_2 structure, then as the pressure is increased there is a phase transition to the O2 structure, and at very high pressures there is a phase transition from the O2 structure to a CP structure.

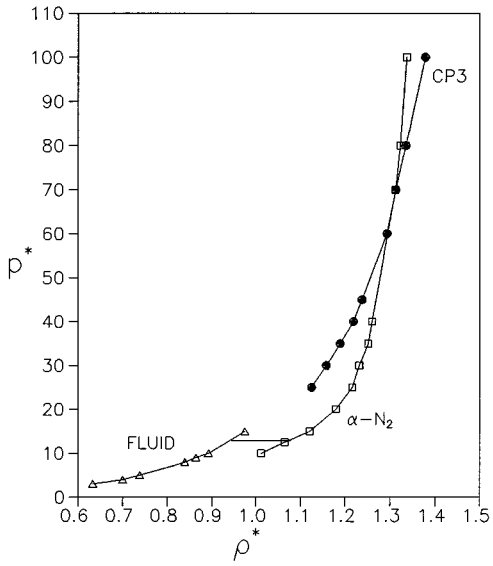

FIG. 6. Equation of state for HDQ with $L^*=0.6$ and $Q^{*2}=0.5$. Notation as in Fig. 3.

Figure 9 summarizes all the results obtained for hard dumbbells with $L^*=0.8$. For very small quadrupole moment the fluid freezes into the CP3 structure, at moderate quadrupole moment freezing occurs into the O2 structure and at large quadrupole moment freezing into the α-N_2 phase occurs. Once again at high pressures the CP3 structure is the stable one. In Fig. 9 estimated values of $Q^2/(kT_md^5)$ for CO_2 and I_2 are shown obtained from experimental data[5] and reasonable estimation of d[26,30] assuming an elongation of $L^*=0.8$ for these molecules. The quadrupolar hard dumbbell model explains the freezing of a molecule like I_2 into an orthorhombic structure or one like CO_2 into the α-N_2 structure. Moreover for CO_2 it predicts a transition from the α-N_2 to an orthorhombic structure in agreement with recent experimental results.[31]

For all the elongations considered in this work the α-N_2 phase was the stable phase at freezing when the quadrupole moment was sufficiently high. This is due to the fact that the α-N_2 is the more favorable structure for quadrupolar interactions. The most favorable relative orientation between a pair of quadrupoles is the so-called T configuration.[30] The α-N_2 structure allows a large number of pair of molecules to have this T configuration.

IV. CONCLUSIONS

Solid–fluid equilibrium of quadrupolar hard dumbbells has been determined by Monte Carlo computer simulation for a number of elongations and values of the quadrupole moment. The principal findings of this work are as follows.

(i) Short molecules with moderate values of the quadrupole moment freeze into a plastic crystal phase. At higher

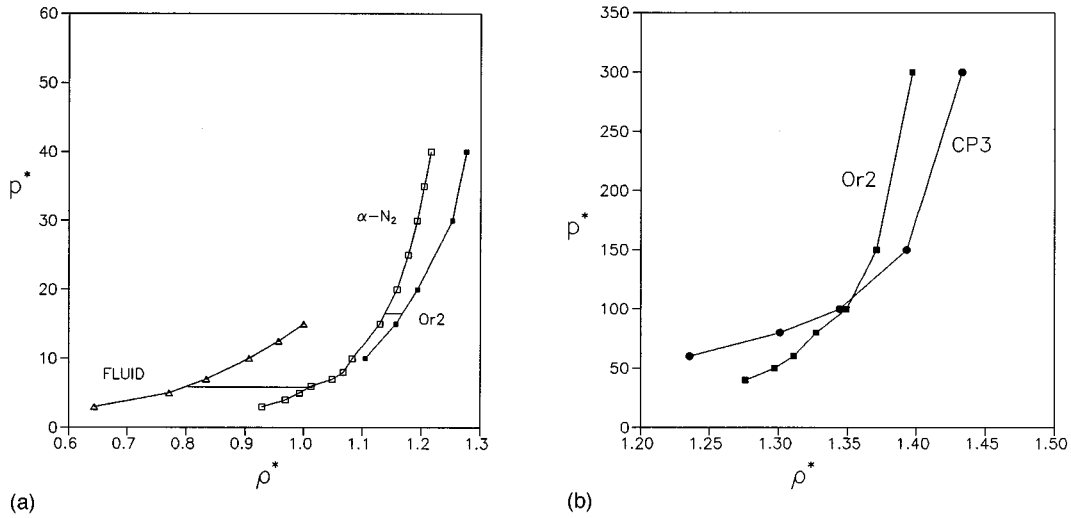

FIG. 8. Equation of state for HDQ with $L^*=0.8$ and $Q^{*2}=1$. Symbols stand for MC results: triangles (fluid phase); open squares (α-N_2); filled squares (O2); circles (CP3). Tie lines correspond to the fluid to α-N_2 and to the α-N_2 to O2 transitions. (a) Low pressure results, (b) high pressure results.

pressures the plastic crystal phase is unstable with respect to the α-N_2 solid and at very high pressures the α-N_2 structure becomes unstable with respect to a base centered monoclinic structure that provides the highest packing density for hard dumbbells.

(ii) Short molecules with large quadrupole moment freeze into the α-N_2 phase. This becomes unstable with respect to a monoclinic close packed structure at higher pressures.

(iii) More elongated molecules freeze into the monoclinic structure for small quadrupole moment, into an orthorhombic structure for moderate quadrupoles, and into an α-N_2 structure for large quadrupoles. At sufficiently high pressure the stable phase is always a monoclinic close packed structure.

(iv) The quadrupole moment is responsible for the appearance of the α-N_2 and orthorhombic structures into the phase diagram of hard dumbbells.

(v) The quadrupolar hard sphere system exhibits only solid–fluid equilibrium, with the fluid density becoming quite low for high quadrupole moment. Such behavior is also expected for the HDQ models.

(vi) Freezing into the α-N_2 structure is accompanied by a relatively large fractional density change on freezing. The is consistent with experimental results for CO_2 and acetylene.

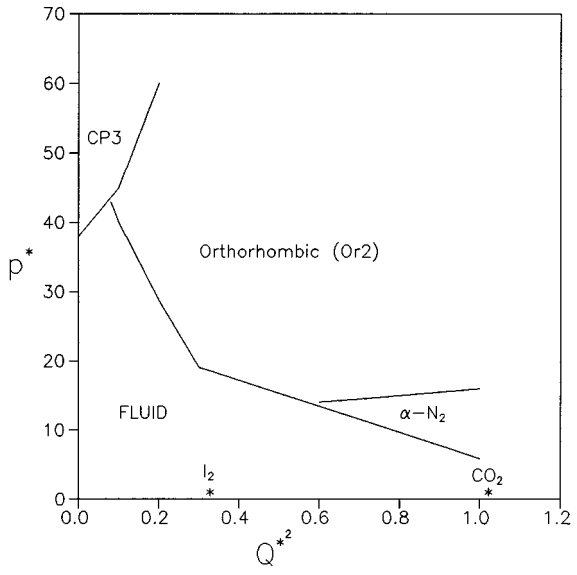

FIG. 9. Phase diagram for quadrupolar hard dumbbells with $L^*=0.8$ for several values of $Q^{*2}=Q^2/(kTd^5)$. Lines correspond to first order phase transitions. Approximate values for Q^{*2} for I_2 and CO_2 at the triple point are shown.

The stable solid phase at freezing for quadrupolar hard dumbbells is shown schematically in Fig. 10 as a function of the molecular elongation and quadrupole moment. Figure 10 also includes the results of our previous work[2] on nonpolar hard dumbbells. The boundaries marked on Fig. 10 are only qualitative estimates made on the basis of our simulation results. There are a number of qualitative similarities between Fig. 10 of this work and Fig. 5 of the paper by English and Venables[30] which was based on calculations of the static lattice energy for the Lennard-Jones diatomic plus quadrupole potential. The regions of stability of the orthorhombic and α-N_2 structures are quite similar. The most important differences arise from the appearance of a plastic crystal phase for mildly anisotropic molecules and that of the close packed monoclinic structures which are the stable structures for hard dumbbells in the high pressure limit irrespective of the quadrupole moment. Also O2 rather than O1 appears as the stable orthorhombic structure for the HDQ model.

Figure 10 can help in our understanding of the stable phases at freezing found for several substances such as the rare gases, the halogens, N_2, O_2, CO_2, and acetylene. As anticipated by Kihara[6] shape and polar forces appear as the most important factors determining solid structure. Of course

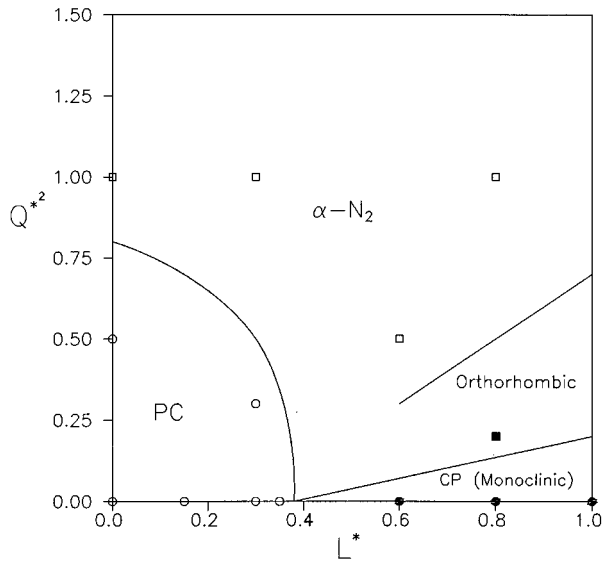

FIG. 10. Schematic diagram of the stable solid phases at freezing for quadrupolar hard dumbbells as a function of L^* and Q^{*2}. Symbols represent the systems studied in this work and in our earlier work for HD: Open circles—PC; filled circles—CP3; open squares α-N_2; filled squares—O2. Solid lines divide the regions where each type of solid is expected to be stable at freezing. These lines are shown only as a guide and precise determination of the domains was not made.

dispersion forces are also important in the determination of solid structure and the model used in this work is too simple to describe all features found in experimental studies of linear molecules. Nevertheless, our results suggest that general trends in the solid–fluid equilibria of quadrupolar linear molecules are already captured by the simple quadrupolar hard dumbbell model.

ACKNOWLEDGMENTS

This work has been supported at the Universidad Complutense, Madrid, by Project No. PB91-0364 of the Spanish DGICYT (Direccion General de Investigacion Cientifica y Tecnica) and at the University of Massachusetts by the U.S. Dept. of Energy under Contract No. DE-FG02-90ER14150.

[1] S. J. Singer and R. Mumaugh, J. Chem. Phys. **93**, 1278 (1990).
[2] C. Vega, E. P. A. Paras, and P. A. Monson, J. Chem. Phys. **96**, 9060 (1992).
[3] C. Vega, E. P. A. Paras, and P. A. Monson, J. Chem. Phys. **97**, 8543 (1992).
[4] E. P. A. Paras, C. Vega, and P. A. Monson, Molec. Phys. **79**, 1063 (1993).
[5] C. G. Gray and K. E. Gubbins, *Theory of Molecular Fluids* (Oxford U.P., New York, 1984).
[6] T. Kihara, Adv. Chem. Phys. **20**, 1 (1971); T. Kihara, Acta Cryst. A **31**, 718 (1975).
[7] S. J. Smithline, S. W. Rick, and A. D. J. Haymet, J. Chem. Phys. **88**, 2004 (1988).
[8] J. D. McCoy, S. Singer, and D. Chandler, J. Chem. Phys. **87**, 4853 (1987).
[9] E. P. A. Paras, C. Vega, and P. A. Monson, Mol. Phys. **77**, 803 (1992).
[10] W. W. Wood, J. Chem. Phys. **48**, 415 (1968).
[11] D. A. Young, *Phase Diagrams of the Elements* (University of California, Berkeley, 1991).
[12] R. L. Collin, Acta Cryst. **5**, 431 (1952).
[13] B. Vonnegut and B. E. Warren, J. Am. Chem. Soc. **58**, 2459 (1936).
[14] M. Parrinello and A. Rahman, Phys. Rev. Lett. **45**, 1196 (1980).
[15] S. Yashonath and C. N. R. Rao, Mol. Phys. **54**, 245 (1985).
[16] D. Frenkel and A. J. C. Ladd, J. Chem. Phys. **81**, 3188 (1984).
[17] D. Frenkel and B. M. Mulder, Mol. Phys. **55**, 1171 (1985).
[18] J. A. C. Veerman and D. Frenkel, Phys. Rev. A **41**, 3237 (1990).
[19] W. G. Hoover and F. H. Ree, J. Chem. Phys. **49**, 3609 (1968).
[20] P. Bolhuis and D. Frenkel, Phys. Rev. Lett. **72**, 2211 (1994).
[21] M. H. J. Hagen, E. J. Meijer, G. C. A. Mooij, D. Frenkel, and H. N. W. Lekkerkerker, Nature **365**, 425 (1993).
[22] N. W. Ashcroft, Nature **365**, 387 (1993).
[23] B. J. Alder, W. G. Hoover, and D. A. Young, J. Chem. Phys. **49**, 3688 (1968).
[24] J. E. Lennard-Jones and A. F. Devonshire, Proc. R. Soc. London **163**, 53 (1937).
[25] R. C. Reid, J. M. Prausnitz, and B. E. Poling, *The Properties of Gases and Liquids* (MacGraw-Hill, New York, 1987).
[26] M. Bohn, J. Fischer, and F. Kohler, Fluid Phase Equilibria **31**, 233 (1986).
[27] T. Boublik, J. Chem. Phys. **87**, 1751 (1987).
[28] E. J. Meijer, D. Frenkel, R. A. LeSar, and A. J. C. Ladd, J. Chem. Phys. **92**, 7570 (1990).
[29] T. Sugawara and E. Kanda, Sci. Rep. Res. Inst. Tohoku Univ. Ser. **4**, 607 (1952).
[30] C. A. English and J. A. Venables, Proc. R. Soc. London, Ser. A **340**, 57 (1974).
[31] K. Aoki, H. Yamawaki, M. Sakashita, Y. Gotoh, and K. Takemura, Science **263**, 356 (1994).